 doi:10.20944/preprints202003.0439.v1

Article

Morphological changes in H1299 human lung cancer cells following Millimeter-wave irradiation

Konstantin Komoshvili[2], Tzippi Becker[1], Jacob Levitan[2], Asher Yahalom[3], Boris Kapilevich[3], Ayan Barbora[1, 2] and Stella Liberman- Aronov[1*]

[1] Department of Molecular Biology, Ariel University, Ariel, Israel.
[2]...Department of Physics, Ariel University, Ariel, Israel.
[3] Department of Electrical & Electronic Engineering, Ariel University, Ariel, Israel.

[*] Correspondence: stellar@ariel.ac.il; Tel.: (972) 3-937-1431 (Israel)

Featured Application: Millimeter-wave irradiation therapy for noninvasive treatment of human non-small cell lung cancer (NSLC).

Abstract: Efficiently targeted cancer therapy without causing detrimental side effects is necessary for alleviating patient care and improving survival rates. This paper presents observations of morphological changes in H1299 human lung cancer cells following MMW irradiation (75 – 105 GHz) at a non-thermal power density of 0.2 mW/cm^2, investigated over 14 days of subsequent physiological incubation following exposure. Microscopic analyses of physical parameters measured indicate MMW irradiation induces significant morphological changes characteristic of apoptosis and senescence. The Immediate short-term stress responses translate into long-term effects, retained over the duration of the experiment(s); reminiscent of the phenomenon of Accelerated Cellular Senescence (ACS) achieving terminal tumorigenic cell growth. Further, results were observed to be treatment-specific in energy (dose) dependent manner and were achieved without the use of chemotherapeutic agents, ionizing radiation or thermal ablation employed in conventional methods; thereby overcome associated side effects. Adaptation of the experimental parameters of this study in clinical oncology concomitant with current developmental trends of non-invasive medical endoscopy alleviates MMW therapy as an effective treatment procedure for human non-small cell lung cancer (NSLC).

Keywords: non-ionizing radiation; lung cancer; millimeter waves; cell morphology; 75-110 GHz

Preprints (www.preprints.org) | NOT PEER-REVIEWED | Posted: 30 March 2020 doi:10.20944/preprints202003.0439.v1

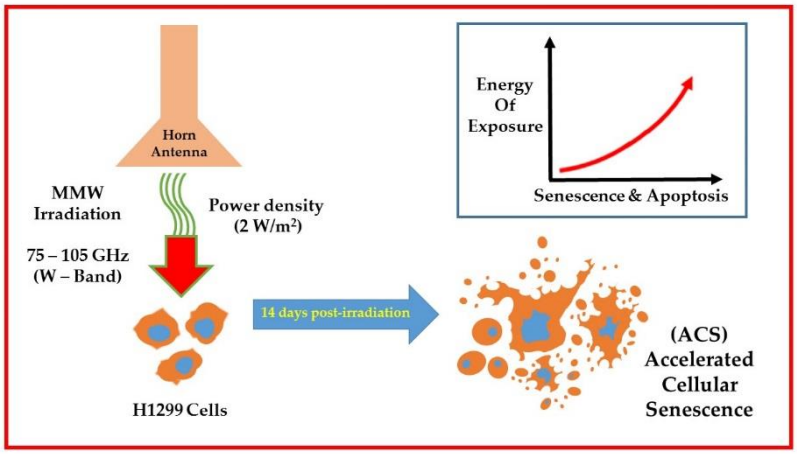

Graphical Abstract

1. Introduction

Lung cancer is the leading cause of cancer deaths among men and second among women worldwide [1]. The 5-year survival rates are very low, ranging from 15.6% in the USA to as low as 8.9% in Europe, China and developing countries [1]. Lung cancer is histologically categorized as small cell lung cancer (SCLC) and non-small cell lung cancer (NSCLC). Arising from epithelial cells [2] NSCLC accounts for 80-85% of all cases. Common types of treatment methods include surgery, radiotherapy and chemotherapy [2]. However, most conventional treatments to control tumor growth are often reported to give rise to many other detrimental side effects [3, 4] due to cross reactions of chemotherapy drugs with healthy tissue and use of ionizing radiations in radiotherapy. Further, post-treatment supportive care after chemotherapy is reported to go only so far as to improve survival rates very slightly [5]. Therefore, development of new and innovative therapies allowing efficient targeting of tumour growth without giving rise to unfavourable after effects is necessary to improve survival rates and alleviate patient care.

Millimeter waves (MMW) classified as non-ionizing radiation are electromagnetic fields (EMF) of extremely high frequencies (30-300 GHz) with corresponding wavelengths of 10 - 1 mm. With relatively low photon energy of 0.0004 eV (1 eV = 1.6 × 19 J), MMW are unable to destroy inter-atomic bonds [6]; but capable of exciting rotational, torsional and longitudinal vibration modes of molecules, resulting in heating. Guidelines of the International Commission on Non-Ionizing Radiation Protection (ICNIRP) stipulates measurement of power density (PD) using units of W/m^2 for exposure of biological tissue to MMW irradiation [7]. The ICNIRP recommends limiting power density within 200 W/m^2 in order to limit adverse thermal effects on biological tissue. MMW irradiation up to a maximum power density of 5 mW/cm^2 have been shown to cause biophysical and biological effects without promoting genotoxicity and adversely increasing cell temperature (non-thermal effects) [8].

MMW irradiation leads to both activation and/or inhibition of cell growth [9 - 11], changes of organelle structures and cell membrane permeability [6, 12, 13], alterations of DNA, RNA and proteins; and the activation or inhibition of signal transduction mechanisms [14 - 16]. Such observed effects have led to a growing interest in applying non-thermal effects of MMW irradiation to target and destroy cancer cells. Previous work from our group reported non-thermal effects of MMW irradiation on human lung cancer cells [17]. In this study, we characterized the associated morphological changes using physical parameters of cell dimensions in order to better understand the mechanism of the radiation effect on the cell and thus optimize MMW irradiation therapy to treat human non-small cell lung cancer (NSLC). For this purpose, H1299 human lung cancer cells were exposed to MMW

Preprints (www.preprints.org) | NOT PEER-REVIEWED | Posted: 30 March 2020 doi:10.20944/preprints202003.0439.v1

irradiation in the range of 75 – 105 GHz within a stipulated non-thermal range of 2 W/m^2. Irradiation was performed under 2 minutes and 4 minutes exposure regimes in order to determine the energy dependence of the observed effects. After irradiation, cells were incubated under physiological conditions and their physical dimensions/parameters analyzed over a period of 14 days to identify immediate and prolonged effects. The dielectric properties of the cell carrier vessels (Petri dishes) and the nutrition medium (RPMI 1640) were characterized prior to irradiation of the cell samples.

2. Materials and Methods

2.1. Cell culture

Human lung cancer cells, H1299 (also known as NCI-H1299 or CRL-5803) were generously provided by Professor Uri Alon of the Weizmann Institute (Rehovot, Israel). Cells were cultured in RPMI 1640 medium (Biological Industries, Beth Ha'emek, Israel) supplemented with 10% fetal bovine serum (FBS), 1% penicillin - streptomycin (Sigma, St Louis, MO, USA), and 2mM glutamine (Biological Industries, Beth Ha'emek, Israel). Cells were incubated at 37 °C with 5% CO_2 supply. The proliferation rate of all cells were similar with a doubling time of 12 to 14 hours, under these conditions.

2.2. Irradiation setup

An experimental setup similar to the one described by Homenko et al. [18] was used, modified for operation in the full W-band (75-110 GHz). It consisted of a Scanning 8360B Series Swept Signal Generator and an 8757D Scalar Network Analyzer (Agilent™). The sweeping frequency synthesizer was operated at 10-20 GHz serving as an input into a solid-state multiplier. A multiplying factor of 6 generated an output signal of 75-110 GHz corresponding to wavelengths (λ) of 4 – 2.725 mm. The waves transmit through the reflectometer connected to two directional couplers arranged facing each other in opposite directions. The setup was calibrated for the reflection mode and the reflection coefficient measured on the analyzer. MMW were partly reflected, partly absorbed and partly transmitted through the sample. The reflection coefficient was estimated in decibels (dB) as a logarithmic ratio:

$$s = 10\log_{10}\left(P_r / P_0\right) \quad (1)$$

where P_r and P_0 are the reflected and incident powers, respectively. Cell irradiation was performed in a sweeping regime from 75 to 110 GHz over 2,000 steps in frequency. One run over this range took 200 ms.

2.3. Penetration of MMW through Petri dish and cell growth medium

Responses of five empty Petri dishes from different manufacturers to low-intensity MMW irradiation was recorded and compared. Petri dishes from Nunc™ (Thermo Fisher Scientific®) showed the best results in terms of uniformity and good transparency, hence all experiments were performed using these Petri dishes. An empty dish was placed over the lower antenna and the reflected and transmitted signals were measured in the sweeping regime from 75 to 110 GHz. Then, using a micropipette with an accuracy of 1 µL several doses of 0.25 mL RPMI 1640 medium were successively added to obtain volumes of 0.5, 0.75, 1.00, 1.25, 1.50, 1.75 and 2.00 mL. These volumes correspond to an RPMI 1640 medium layer thickness d = 0.52, 0.80, 1.03, 1.30, 1.56, 1.82 and 2.08 mm in the petri dish. For each new volume, a new sweeping run was executed. From the obtained measurements in dB presented by equation (1) the normalized reflected and transmitted powers were calculated by

$$P / P_0 = 10^{s/10} \quad (2)$$

where P is either the reflected or transmitted power and P_0 the incident power respectively.

Preprints (www.preprints.org) | NOT PEER-REVIEWED | Posted: 30 March 2020 doi:10.20944/preprints202003.0439.v1

2.4. Exposure conditions

A pyramidal horn antenna, model SGH-10 (Millitech Inc.) with aperture dimensions of 20 mm x 25 mm was used to irradiate the test samples. 1 mW incident power was used for all irradiation experiments, translating to a power density of 2 W/m^2 (0.2 mW/cm^2). Every single experiment involved irradiation of approximately $2x10^5$ cells per dish when the cells reached 30% confluence. To investigate MMW effects on morphology, cells were irradiated under specific time regimes. Each experiment lasted up to 14 days. On day 1 cells were irradiated with MMW for 2 minutes (Group a) or 4 minutes (Group b) respectively. Following irradiation, cells were incubated at 37 ºC with 5% CO_2 for up to 14 days. Slides of cell samples were prepared at specific time points - Day 1 (90 minutes after irradiation), Day 7 and Day 14. Digital images of live cells were taken using a light microscope on Day 1, Day 7 and Day 14 respectively. In order to rule out morphological changes due to cell proliferation and were not specific to MMW irradiation, two controls were used: 1) cells that underwent the same procedures but were not irradiated and 2) cells that were left untouched in the incubator. Control samples were assessed at the same time points as the irradiated cells (i.e., at Day 1, Day 7 and Day 14 of the experiment).

2.5. Microscopy and image processing

MMW effects on the morphology of the cells were examined using a Nikon fluorescent microscope (Nikon Instruments Inc., Melville, NY) at a magnification of 200x. Images were captured using a digital color-chilled 3CCD camera (Hamamatsu, Bridgewater, NJ) and visualized using the NIS Elements microscope software program (Nikon Instruments Inc.). Image processing and analysis were performed using ImageJ (Java-based image processing program developed at the National Institutes of Health, MD). Parameters of cell area, cell circularity and Feret's diameter were evaluated for irradiated and control samples. 8000 to 10000 cells were examined in each experiment. Every experiment was repeated four times.

2.6. Statistical analysis

Statistical analyses was performed using the GraphPad Prism program (GraphPad Software, La Jolla, CA). Multivariate analysis of variance (MANOVA) and Tukey-Kamer multiple comparison test were used for comparing the irradiated cells with the control groups; and for comparing the changes in irradiated cells at different exposure times. The means of the measured parameters (area, circularity and Feret's diameter) for the respective groups were considered equal for the null-hypothesis in all cases. A P-value <0.05 was considered significant for rejecting the null-hypothesis for all experiments.

3. Results

3.1. Millimeter waves can penetrate through Petri dishes

In order to characterize their dielectric properties Petri dishes were irradiated from above (Figure 1a). MMW reflected from the petri dishes were detected. The range of reflected power for frequencies 75 – 100 GHz was found to be with a reduction of -15 dB to -35 dB with respect to the incident power (corresponding to 3 – 0.03 % of incident power) respectively (Figure 1b). The frequency spectrum of the reflected signal of all tested petri dishes coincided.

Preprints (www.preprints.org) | NOT PEER-REVIEWED | Posted: 30 March 2020 doi:10.20944/preprints202003.0439.v1

Figure 1

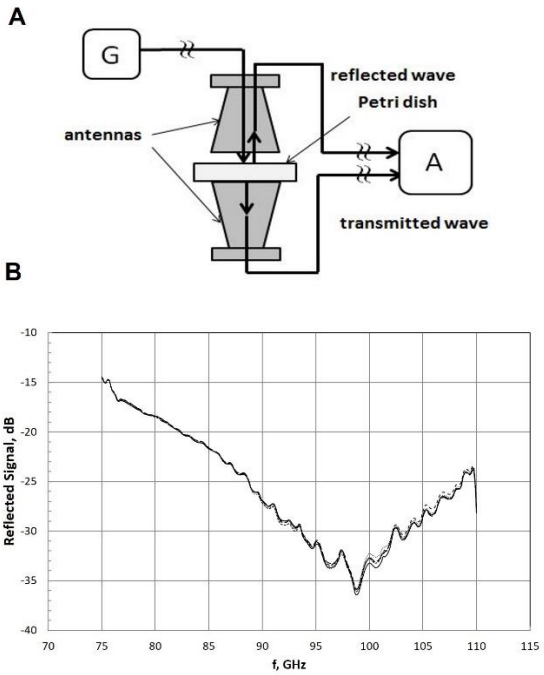

Figure 1. Illustration of the irradiation setup (**A**). G represents the millimeter wave generator and A represents the network signal analyzer. The scalar network analyzer measured the waves reflected partly into the upper antenna and transmitted partly into the lower antenna. Characterization of the dielectric properties of petri dishes (**B**). The graph represents frequency spectra of the reflected signal of five empty Petri dishes (Nunc™, Thermo Fisher Scientific). In total, 43 dishes were tested with the same results.

3.2. Millimeter waves transmit through RPMI 1640 cell growth medium without generating thermal heat

The wavelength of MMW is comparable to the layer thickness of the RPMI 1640 medium (2- 3 mm) used. Additionally, MMW undergo multiple reflections in the RPMI 1640 medium. Reflected waves (from the sample) are a combination (interference) of waves reflected from the surface of the nutrition media, the bottom of the dish, and from the cells under investigation. Single (discrete) frequency irradiation regime requires fine adjustments of the distance between sample and antenna in order to obtain conditions of constructive interference. In contrast, irradiation under a continuous sweeping of frequency allows for repeated wavelength changes over each run providing conditions of constructive and destructive interference successively. This is advantageous and overcomes the necessity for fine adjustments. Thus, at least during half the duration of a single run efficient power delivery is obtained. Therefore, all experiments were conducted in the sweeping regime.

Although several studies have evaluated the real and simulated dielectric constant of RPMI medium for frequencies up to 72 GHz [19, 20], such data is lacking in the MMW W-band range used in our experiments (75 – 105 GHz). Hence, we tested the amount of energy that gets reflected from and penetrates through RPMI 1640 cell growth medium supplemented with 10% fetal bovine serum (FBS) and 1% penicillin/streptomycin. This basic medium consists of about 40 nutrition ingredients including various types of proteins present in FBS, diluted in water. The dependence of the reflected and the transmitted signals (normalized to the antenna emitting power $P_0 \approx 1$ mW) on the thickness of RPMI 1640 medium layer thickness in the Petri dishes was studied for different frequencies (Figure 2a). The ratio of the transmitted and incident power decreases as the thickness of the media increases. For a medium layer thickness of 2 mm, the ratio decreases by a factor of 10^{-4}–10^{-5}. In absolute values, this ratio

Preprints (www.preprints.org) | NOT PEER-REVIEWED | Posted: 30 March 2020 doi:10.20944/preprints202003.0439.v1

corresponds to 10-100 nW of power reaching the population of cells adhered at the bottom of the dish. In other words, maximum incident power is absorbed in an RPMI 1640 medium layer thickness of 2 mm. As the medium consists mostly of water, we used the heat capacity of water to estimate the temperature increase during irradiation using

$$\Delta T \cong P_T t / (c\, m) \qquad (3)$$

where t is the exposure time, c the heat capacity (4.18 J/g·K) and m the sample mass (1.50 g). This estimation is based on the assumption that the penetrating power decreases exponentially with depth due to increased absorption of incident energy. Our calculations predict a temperature rise of no more than 0.2 - 0.4 K for 2 - 4 minutes of irradiation of samples immersed in 2 mL of RPMI 1640 medium. Further, temperature of the medium during irradiation was measured to be in the range of 24 – 26 °C.

Figure 2

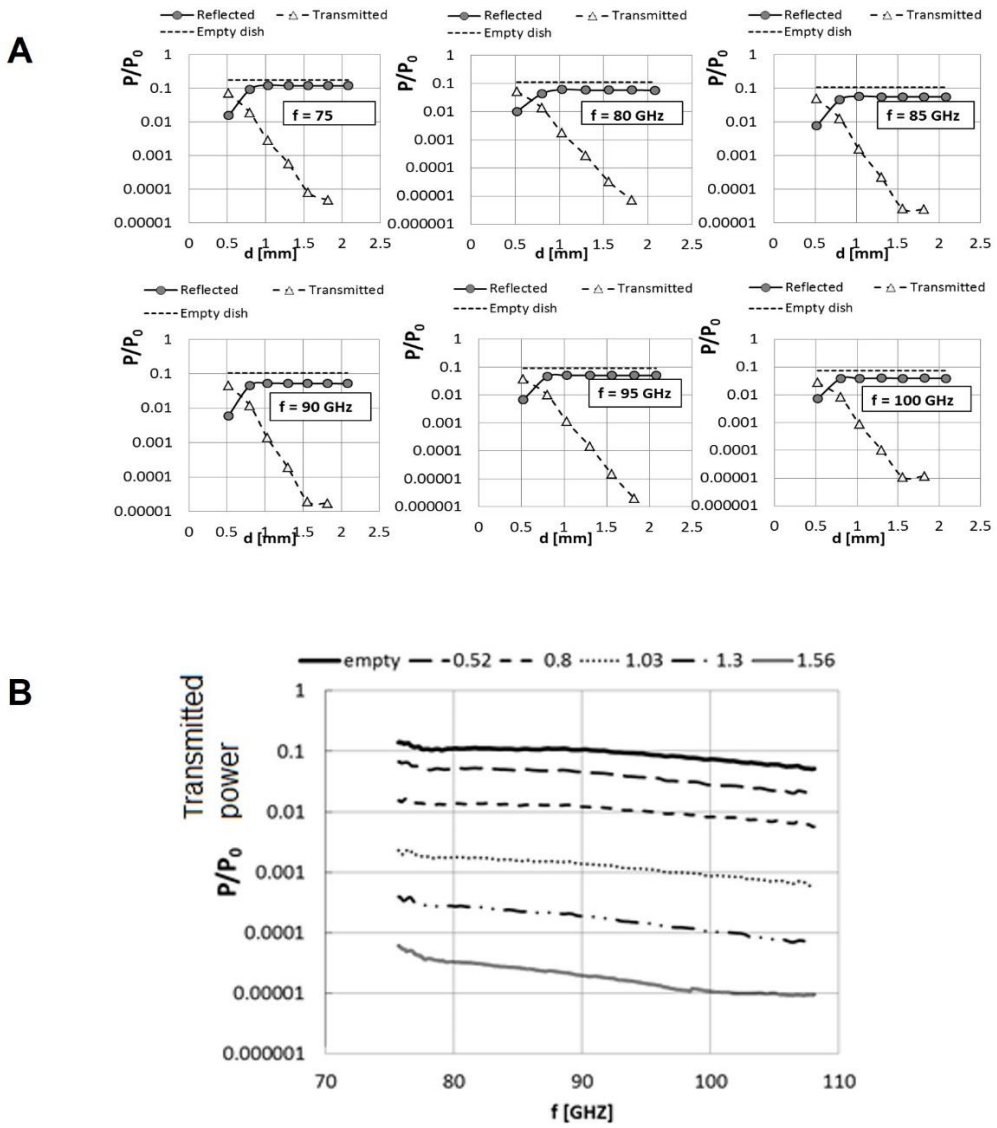

Figure 2. Dependence of the reflected and the transmitted signals on the level of RPMI 1640 medium layer thickness (**A**). Signals were evaluated for different frequencies ranging from 75 to 100 GHz. For the empty dish, only transmitted signal and not the reflected signal is presented. Shown is one representative sample of seven dishes that were irradiated for each frequency. Exposure times were a few seconds and the temperature of the medium was measured to be 24 – 26 °C. Dependence of the

 doi:10.20944/preprints202003.0439.v1

transmitted power through the Petri dish on frequency of irradiation (**B**). The signals were normalized to the antenna emitting power $P_0 \approx 1$ mW on an empty dish.

In order to maximize power delivery to cells under irradiation and minimize attenuation loss arising from absorption by culture media, we examined the full frequency spectra (75 – 105 GHZ) of the transmitted signals penetrating through petri dishes with different RPMI 1640 layer thicknesses (Figure 2b). -7.6 dB is the free space path loss (FSPL) for the 25 mm separation distance between the two +24 dB gain antennas of our setup, as detailed above (ref. Figure 1). Insertion of an empty dish increased the loss of the initial power by approximately 70% due to attenuation by the polystyrene of the dish (Figure 2b). The transmitted power level in the empty dish decreased by one order of magnitude with introduction of culture medium, corresponding to an attenuation of about -10 dB. The results indicate an RPMI layer thickness of 0.5 mm as the best working range, translating to a volume of 0.5 ml of RPMI 1640 medium. Maximum transmitted power is allowed to reach the suspended cells upon irradiation at 75 – 105 GHz in this range. Therefore, all subsequent experiments were performed using this volume of culture media.

3.3. MMW irradiation changes morphology and size of H1299 cancer cells

H1299 lung cancer cells were irradiated with millimeter waves and subsequently were incubated under physiological conditions, before further evaluation. Analyses of irradiated and control cells were conducted on Day1 (90 minutes post irradiation), Day 7 and Day 14 (Figure 3a). Exposure power density was maintained at 0.2 mW/cm^2 over the duration of exposure; much below the maximum permissible exposure of 1 mW/cm^2, as stipulated by the US Federal Communications Commission [21 - 25]. This power density in association with the estimates and measurements of temperature increase mentioned above, allowed for ruling out thermal effects arising from this irradiation regime. Therefore, the effects observed experimentally were considered non-thermal in nature. Prior to irradiation, cell morphology was examined by microscopy. H1299 cells were observed to be adherent flattened cells with a thickness of less than 5 μm; indicating measurements of cell area are representative their actual size.

Prior to quantifying the changes in their morphology following irradiation, cells were divided into 10 subgroups based on their area size (500 μm^2 each) (Figure 3b). Number of cells for each subgroup was determined by counting during imaging observation in the light microscope (see methods). The square root of the observed top-view area was found to be 25 - 30 μm for the average population. Non-irradiated control cells were observed to be in interphase with polygonal, slightly elongated or oval forms. Majority of these cells presented areas in the range of 500 - 3000 μm^2 (Figure 3b). Dividing cells with areas ranging from 2500 - 3500 μm^2 constituted about 3 - 5% of the population. Huge (giant) polyploid cells, about 2.5 - 3.5 times larger than the main cell population with areas ranging from 3500 - 5000 μm^2 constituted about 1 - 2% of the cell population (Figure 3b). The observations showed that H1299 cell populations present a heterogeneous morphology corresponding to the physiological status of the cells in their cell cycle states; concomitant with studies reporting cancer cell diversity and genetic instability [26]. Changes in cell morphology were observed after 7 and 14 days following irradiation (Figure 3c). Pro-apoptotic cells characterized by shrinkage and fragmentation [27] constituted 1 – 3 % of the cell population. Further, 10 % of the population developed protrusions two to three times longer than the cell body (Figure 3c). The percentage of polyploid (giant cells) were also increased, suggesting induction of senescence [28, 29].

 doi:10.20944/preprints202003.0439.v1

To determine the dependence of observed morphological changes on the energy delivered by MMW exposure, cells were irradiated under two separate exposure regimes of 2 minutes and 4 minutes respectively. Depending on the frequency, a single run at a maximum incident power of 1 mW incident power was almost completely attenuated in 2 mL of RPMI 1640 medium, reaching a level of about P ≈ 1 μW at the bottom of the petri dish (ref. Figure 2). In this regime, the energy delivered to the bottom of the dish was 200 nJ (1 μW × 200 ms). Exposure for 2 minutes translates into 600 runs (i.e. 120 s divided by 0.2 s of a single run), providing 120 μJ of energy. Similarly, 4 minutes of exposure translates into 240 μJ of energy. Since $2x10^5$ cells were irradiated in every single experiment, the estimates detailed above give an average energy dose of of 0.6 nJ and 1.2 nJ per cell for 2 and 4 minutes exposure regimes respectively. Irradiated cell samples were analyzed for long-term (7 or 14 days) effects following irradiation after subsequent physiological incubation. Cells observed and analyzed on the same day of irradiation (90 minutes after exposure) were taken as control to characterize immediate short-term effects (ref. Figure 3a). Under the 2 minutes exposure regime, samples analyzed on the same day of irradiation did not show any significant change (Figure 3d) in the population as compared to control non-irradiated cells (ref. Figure 3c). However, 7 days post-irradiation under this regime presented a slight but significant increase in the number of huge polyploid cells (ranging 3000 - 4000 μm^2 in size) (Figure 3d). These cells were observed to be greatly enlarged in size (ref. Figure 3c). Additionally, 14 days post- irradiation under this regime resulted in a dramatic shift of the entire cell population turning into giant polyploid cells (ranging 3000 – 4000 μm^2 in size) (Figure 3d); indicative of induced senescence [28, 29]. In contrast, the 4 minutes exposure regime led to the population of irradiated cells splitting into two groups (Figure 3e) as compared to the control non-irradiated cells (ref. Figure 3c). Under this exposure regime, the population of cells analyzed on the same day of irradiation showed shrinkage in size (ranging 0 – 500 μm^2 in size) (Figure 3e). 7 days post-irradiation under this regime presented a significantly higher number of cells with shrunken size (Figure 3e) indicating that cells were undergoing apoptosis [27]. Further, 14 days following exposure in this regime showed the irradiated cells had split into two groups of population (Figure 3e); notably shrunken cells (ranging 0 – 500 μm^2 in size) and giant enlarged cells (ranging 3000 - 4000 μm^2 in size).

Preprints (www.preprints.org) | NOT PEER-REVIEWED | Posted: 30 March 2020 doi:10.20944/preprints202003.0439.v1

Figure 3

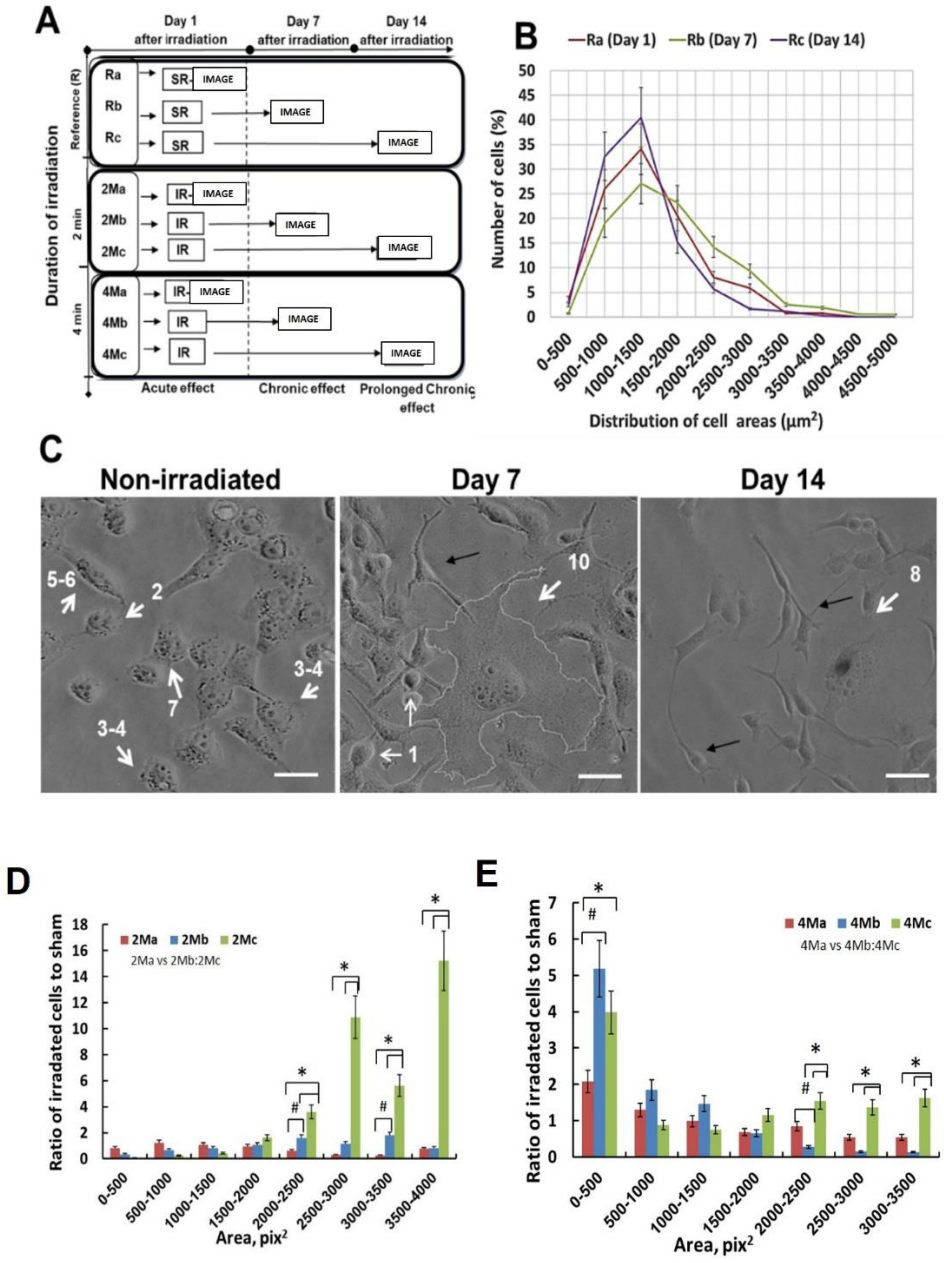

Figure 3. Pictogram of the experimental strategy (**A),** depicting time schedule and analytical conditions (R – Non-irradiated control retained in the incubator, 2M – two minutes, 4M – four minutes. IR – irradiation, SR – Control cells that underwent the same procedures as the irradiated cells without being irradiated, IMAGE – Microscopy and image analysis). Cells were irradiated for two minutes (2M) or four minutes (4M). Image analysis was performed on day 1 (short-term, a), day 7 (long-term, b), or day 14 (long-term, c). Controls were assessed at the same time points as the irradiated cells (i.e., Ra, day 1; Rb, day 7; and Rc, Day 14 of the experiment). Quantification of the distribution of control non-irradiated cell areas (**B**) for day 1 (Ra, red line), day 7 (Rb, green line) and day 14 (Rc, violet line). Cell areas were grouped into 10 intervals (500 μm² each) and the number of cells in each group counted and examined by microscopic observation followed by image analysis of cell sizes using ImageJ program.

 doi:10.20944/preprints202003.0439.v1

Morphological changes of H1299 cells following MMW irradiation (**C**). Prior to irradiation majority of the cells presented polygonal forms (white arrowhead 2-6) and dividing cells constituted 3-5% of the cell population (white arrow 7). Analysis of cell areas 7 days after MMW irradiation revealed 1-3% of pro-apoptotic cells (white arrow 1). 1% of cells showed characteristics of huge (giant) polyploid cells (white arrow 8 and 10). 10% of the cells showed an oval cell morphology with highly elongated protrusions, two to three times longer than the cell itself (black arrow). Bars correspond to 20 μm. Changes in H1299 cell size irradiated under 2 minutes exposure regime (**D**); analyzed on day 1 (2Ma), day 7 (2Mb) and day 14 (2Mc). Cell sizes increased (3000 - 4000 μm^2) significantly following this treatment regime over a long-term period of 7 and 14 days. Changes in H1299 cell size irradiated under 4 minutes exposure regime (**E**); analyzed on day 1 (4Ma), day 7 (4Mb) and day 14 (4Mc). Cell size both decreased (0 – 500 μm^2) and increased (3000 - 4000 μm^2) significantly following this treatment regime immediately (on Day 1) and over a long-term period of 7 and 14 days respectively. 8000 - 10000 cells were analyzed for every single experiment using Image J. Error bars represent the standard deviations of four biologically independent experiments (N = 4); p-values < 0.05 was considered statistically significant with * representing $p < 0.05$ (for a versus c or b versus c) and # representing $p < 0.05$ (for a versus b).

The results indicate that duration of MMW exposure directly determines the extent to which cell morphology is affected. A short 2 minutes exposure does not produce any immediate effects but induces development of enlarged cells, indicative of senescence [28, 29]. In contrast, a 4 minutes exposure regime providing a higher dosage of MMW energy results in both short and long-term effects. Immediately, following exposure in this regime cells are induced to a far greater degree of shrinkage as compared to that under the 2 minutes regime; indicating acute apoptosis [27]. Further, the 4 minutes regime also induces development of enlarged polyploid cells indicative of senescence [28, 29], over a long-term period of 14 days following irradiation.

3.4. MMW irradiation increases cell circularity and Feret's diameter of H1299 cancer cells

In order to ascertain that MMW irradiation induced apoptosis and senescence as indicated by the results above; further stringent parameters were quantified. Specifically, cell circularity and Feret's diameter were measured to determine the extent of the said effects. Circularity values ranging from a least circular shape (value 0) to a perfect circle (value 1) is used to denote the degree of dimensional roundness of an object. Increased cell circularity is a hallmark of apoptosis resulting from cytoplasmic shrinkage and cell fragmentation [30]. Majority (80%) of untreated control cells presented circularity values between 0.5 - 0.8 (Figure 4a). Following MMW exposure, the circularity of irradiated cell populations increased by 1.5 times as compared with that of control untreated cells. The 2 minutes irradiation regime led to a population shift towards a more circular shape (0.8 - 0.9) on day 1 (Figure 4b). 7 days of physiological incubation following exposure in this regime presented cell populations split into two groups. One group retained the circular form (0.8 - 0.9) indicating apoptotic or programmed cell death (PCD) cells and another a less circular form (0.3 - 0.5) than untreated cells, likely to be fragments of already PCD cells which lost their normal form and size. Interestingly, the split in population was retained even after 14 days following irradiation. The 4 minutes irradiation regime resulted in a similar but more marked trend of population shift (Figure 4c). As these effects persisted over day 7 to 14 day of post-irradiation period and were not observed in the untreated control cells, the changes in cell circularity were concluded to be a specific response to MMW irradiation.

Preprints (www.preprints.org) | NOT PEER-REVIEWED | Posted: 30 March 2020 doi:10.20944/preprints202003.0439.v1

Figure 4

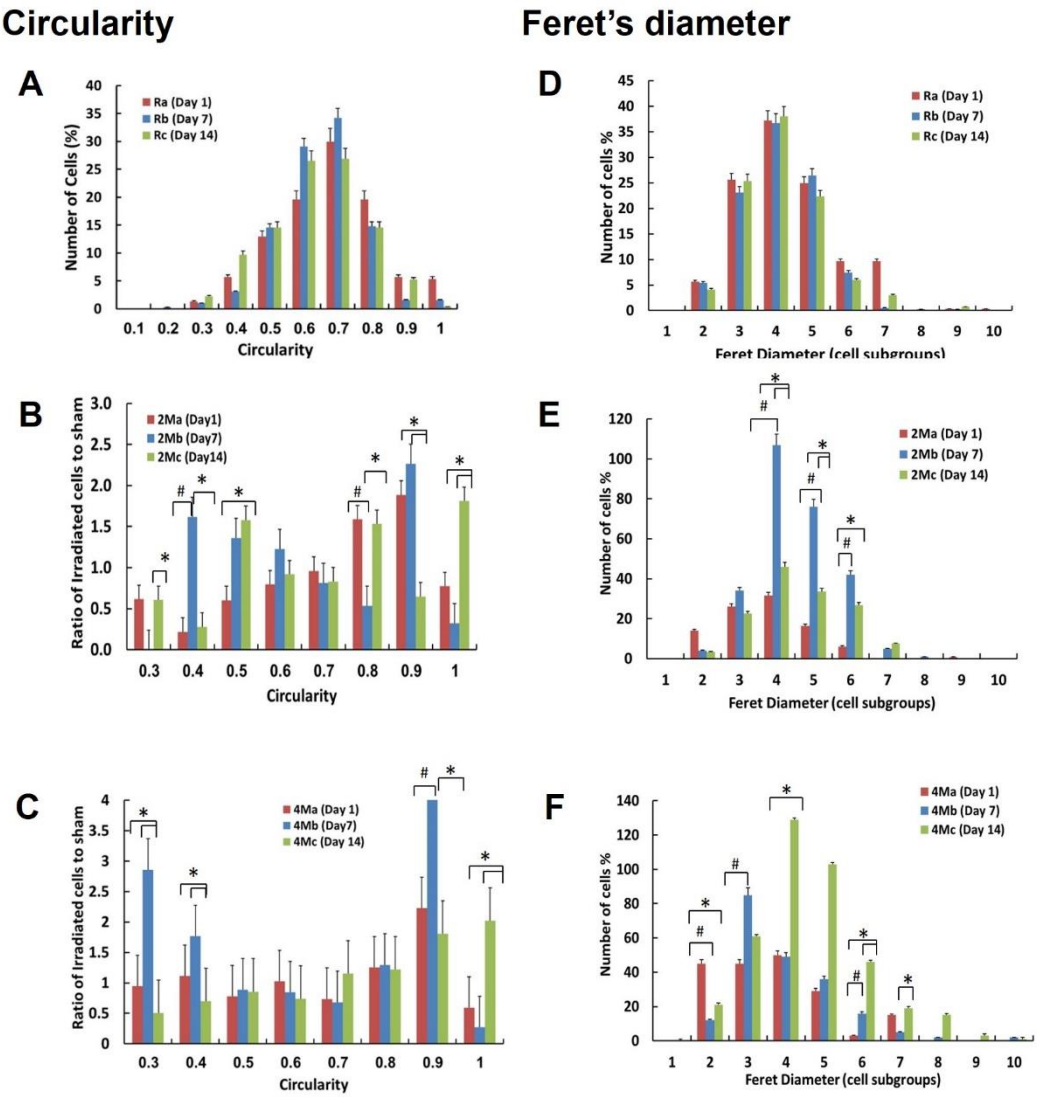

Figure 4. Distributions of cell circularity (**A**-**C**) and Feret's diameter (**D**-**F**) following effects of MMW irradiation; analyzed on Day 1 (red bars), Day 7 (blue bars) and Day 14 (green bars). Values of cell circularity were divided into 10 subgroups and the number of cells in each group counted. The Y-axis represents the ratios of the number of irradiated cells to the number of untreated control cells for the same subgroup. Cell circularity of H1299 cells left untreated (**A**); analyzed on day 1 (Ra), day 7 (Rb) and day 14 (Rc). Cell circularity of H1299 cells irradiated under 2 minutes exposure regime (**B**); analyzed on day 1 (2Ma), day 7 (2Mb) and day 14 (2Mc). Cell circularity of H1299 cells irradiated under 4 minutes exposure regime (**C**); analyzed on day 1 (4Ma), day 7 (4Mb) and day 14 (4Mc). Values of Feret's diameter were divided into 10 subgroups and the number of cells in each group counted. Each subgroup corresponds to 25 μm for all experiments. The Y-axis represents the ratios of the number of irradiated cells to the number of untreated control cells for the same subgroup. Feret's diameter of H1299 cells left untreated (**D**); analyzed on day 1 (Ra), day 7 (Rb) and day 14 (Rc). Feret's diameter of H1299 cells irradiated under 2 minutes exposure regime (**E**); analyzed on day 1 (2Ma), day 7 (2Mb) and day 14 (2Mc). Feret's diameter of H1299 cells irradiated under 4 minutes exposure regime (**F**); analyzed on day 1 (4Ma), day 7 (4Mb) and day 14 (4Mc). 8000 - 10000 cells were analyzed for every single experiment using Image J. Error bars represent the standard deviations of four biologically independent experiments (N = 4); p-values < 0.05 was considered statistically significant with * representing $p < 0.05$ (for a versus c or b versus c) and # representing $p < 0.05$ (for a versus b).

Preprints (www.preprints.org) | NOT PEER-REVIEWED | Posted: 30 March 2020 doi:10.20944/preprints202003.0439.v1

Feret's diameter (FD) measured, as the longest straight line between two points on the periphery of a cell is an important morphological marker of cells undergoing senescence [31]. Larger FD corresponds to longer cellular extensions (i.e. protrusions); and enlarged structurally aberrant cells characteristic of senescence [32]. FD of non-irradiated cells did not change over the experimental time course (Figure 4d). The 2 minutes exposure regime led to a significant increase of FD over 7 days of physiological incubation following irradiation (Figure 4e) and was reversed after 14 days. In contrast, the 4 minutes irradiation regime resulted in an FD increase over 14 days and not 7 days (Figure 4f). These results demonstrate that a significant number of cells changed their shapes and sizes in an energy (dose) dependent manner as a specific response to MMW irradiation. Trigonal, flattened, adherent cells of the control groups changed to oval-shaped cell bodies with long protrusions following MMW exposure treatment.

4. Discussion

Cancer characterizes by an excessive and uncontrolled division of abnormal, malignant cells that display morphological, proliferative, and functional heterogeneity (26). Cell size is an important morphological criterion characterizing the physiological status of a cell. Majority of animal cells are 10-20 μm in diameter and rarely vary more than two folds outside of this range, suggesting that the mechanism for cell size regulation is highly conserved [33]. Changes in H1299 cell morphology following exposure to 75-110 GHz MMW for 2 and 4 minutes irradiation regimes respectively, were examined in this study. Past investigations of MMW irradiation effects on normal and cancer cells had reported distinct non-thermal biological effects using discrete narrow range(s) of frequency with very low energy [12 - 13, 19, 34 - 35]. MMW irradiation of lung cancer cells in the present study led to significant visible morphological changes in cell area, cell circularity and Feret's diameter. These changes were observed on the same day of exposure treatment (short-term effects), as well as over 7 - 14 days post-irradiation (long-term effects). The short-term effects are likely due to regular stress responses following irradiation. However, the long-term effects arise specifically as a result of MMW irradiation and were observed to be retained over the duration of the experiment(s). Senescent cells are known to present an enlarged phenotype as compared to non-senescent cells [36]. This suggests that the dramatic increment of cell size observed under the 2 minutes irradiation regime indicates a population shift towards a higher number of senescent cells induced by MMW irradiation. In contrast, the results from the 4 minutes exposure regime, which delivered a higher dose of MMW energy, indicated induction of apoptosis as well as senescence. These are favorable effects for clinical applications of MMW therapy to control tumor metastasis.

Reports of heterogeneity [26] as well as our results, demonstrate cancer cells maintain generally constant sizes throughout their lifetime. And being highly dynamic can either grow or shrink in size in response to specific conditions via robust and adaptable control mechanisms. Illustratively, alterations of cell morphologies in response to the chemical cancer drug paclitaxel have been observed with similar results [37]. Cancer cell tumorigenicity is associated with cell softening and decrease in cell stiffness arising from cytoskeletal restructuring [38]. Integral membrane proteins mediate this transition of normal cells into cancer cells [39]. Changes in cell shape and size following MMW irradiation in the present study were specific and irreversible, directly corresponding to changes of cell circularity and Feret's diameter. MMW irradiation affects cell growth [9 - 11] by changing organelle structure and cell membrane permeability [6, 12 - 13]. Such interactions lead to the activation and inhibition of signal transduction mechanisms due to MMW interacting with DNA, RNA and Proteins [14 - 16]. Increased membrane stiffness resulting in apoptosis of cells has been shown to correspond to changes in prostate cancer cells responding to anti-neoplastic treatment [40]. These suggest the Accelerated Cellular Senescence (ACS) effect [41] occurring in an energy (dose) dependent manner observed in this study arises from the non-thermal low power density MMW exposure affecting H1299 membrane fluidity.

5. Conclusions

The experimental results of this study suggest MMW irradiation in the frequency range of 75 - 110 GHz (W-band) promote specific morphological changes in H1299 human lung cancer cells in an energy (dose) dependent manner. Effects observed and quantified using physical dimensions/parameters of cell size, circularity and Feret's diameter demonstrate characteristic features of induced apoptosis and senescence following MMW exposure. The phenomenon of Accelerated Cellular Senescence (ACS) [41] wherein cancer cells undergo terminal growth arrest is conventionally achieved by using radiotherapy in conjunction with specific chemotherapeutic agents for targeted blockage of cellular pathways. *In vivo* studies suggest MMW can be used to activate Natural Killer (NK) cells aiding to reduce tumor metastasis [42]. The present study reports apoptosis and senescence of cancer cells without the use of chemotherapeutic agents, ionizing radiation or thermal ablation, thereby overcoming associated side effects [Salvo et al., 2010; Ryan, 2012]. In conjunction with the development of endoscopic methods, MMW irradiation parameters described in this study holds promising potential for the development of non-invasive procedures to treat lung cancer in the future.

Author Contributions: Conceptualization, K. K., A.Y., J.L. and S.L-A.; Methodology, K.K., A.Y., J.L., B.K.; and S.L-A.; Software, K.K., T.B., and S.L-A. Validation, K.K., T.B. and S.L-A.; Formal analysis, K.K.; T.B and S.L-A.; Investigation, K.K., T.B and S. L-A. Resources, K.K., A.Y., J.L. and S.L-A. Data curation, K.K., A.Y. and S.L-A. Writing—original draft preparation, K.K., A.B. and S.L-A. Writing—review and editing, K.K., A.B, A.Y. and S.L-A. Visualization, K.K., T.B and A.B. and S.L-A. Supervision, S.L-A. Project administration, S.L-A. Funding acquisition, K.K., A.Y., J.L. and S.L-A. All authors have read and agreed to the published version of the manuscript.

Funding: This research was funded by Ariel University's Internally Supported Grant (Ariel Center for Applied Cancer Research, ACACR) and the Eva and Henry Fraenkel Foundation (Denmark).

Acknowledgments: We are grateful for the very useful discussions with Prof. H. G. Bohr (Denmark); and for Mr. D. Hardon and Mr. B. Litvak's help in performing the irradiation experiments.

Conflicts of Interest: The authors declare no conflict of interest.

References

1. Dela Cruz CS, Tanoue LT, Matthay RA. Lung cancer: epidemiology, etiology, and prevention. *Clin Chest Med* **2011**, *32(4)*, pp 605–644. DOI: https://www.ncbi.nlm.nih.gov/pubmed/22054876
2. Hann CL, Rudin CM. Management of small-cell lung cancer: incremental changes but hope for the future. *Oncology (Williston Park)* **2008**, *22(13)*, pp 1486-92. DOI: https://www.ncbi.nlm.nih.gov/pubmed/19133604
3. Salvo N, Barnes E, van Draanen J, Stacey E, Mitera G, Breen D, Giotis A, Czarnota G, Pang J, De Angelis C. Prophylaxis and management of acute radiation-induced skin reactions: a systematic review of the literature. *Curr. Oncol.* **2010**, *17(4)*, pp 94-112. DOI: 10.3747/co.v17i4.493
4. Ryan JL. Ionizing Radiation: The Good, the Bad, and the Ugly. *J Invest Dermatol* **2012**, *132(3)*, pp 985-993. DOI: https://www.ncbi.nlm.nih.gov/pmc/articles/PMC3779131
5. [N.M.-A.C. Group] NSCLC Meta-Analyses Collaborative Group. Chemotherapy in addition to supportive care improves survival in advanced non-small-cell lung cancer: a systematic review and meta-analysis of individual patient data from 16 randomized controlled trials. *J. Clin. Oncol.* **2008**, *28*, pp 4617-25. DOI: https://www.ncbi.nlm.nih.gov/pubmed/18678835Ramundo-Orlando A. Effects of Millimeter Waves Radiation on Cell Membrane - A Brief Review. *J Infrared Milli Terahz Waves* **2010**, *31*, pp 1400–1411. DOI: https://link.springer.com/article/10.1007%2Fs10762-010-9731-z
6. [ICNIRP] International Commission on Non-Ionizing Radiation Protection. Guidelines for limiting exposure to Electromagnetic Fields (100 kHz to 300 GHz). *Health Phys*. **2020**, *118(00)*, pp 1-43. DOI: https://www.icnirp.org/cms/upload/publications/ICNIRPrfgdl2020.pdf
7. Yaekashiwa N, Otsuki S, Hayashi S, Kawase K. Investigation of the non-thermal effects of exposing cells to 70-300 GHz irradiation using a widely tunable source. *J Radiat Res* **2018**, *59(2)*, pp 116–121. DOI: https://academic.oup.com/jrr/article/59/2/116/4769636

8. Grundler W, Keilmann F. Sharp Resonances in Yeast Growth Prove Nonthermal Sensitivity to Microwaves. *Phys. Rev. Lett.* **1983**, *5*, pp 1214–1216. DOI: https://journals.aps.org/prl/abstract/10.1103/PhysRevLett.51.1214
9. Hadjiloucas S, Chahal MS, Bowen JW. Preliminary results on the non-thermal effects of 200-350 GHz radiation on the growth rate of S. cerevisiae cells in microcolonies. *Phys Med Biol* **2002**, *47(21)*, pp 3831-9. DOI: https://iopscience.iop.org/article/10.1088/0031-9155/47/21/322
10. Beneduci A. Evaluation of the potential in vitro antiproliferative effects of millimeter waves at some therapeutic frequencies on RPMI 7932 human skin malignant melanoma cells. *Cell Biochem Biophys* **2009**, *55*, pp 25–32. DOI: https://link.springer.com/article/10.1007%2Fs12013-009-9053-8
11. Siegel PH, Pikov V. Impact of low intensity millimetre waves on cell functions. *Electron Lett* **2010**, *46(26)*, pp 70-72. DOI: http://www.thz.caltech.edu/siegelpapers/IET_Dec2010.pdf
12. Shapiro MG, Priest MF, Siegel PH, Bezanilla F. Thermal Mechanisms of Millimeter Wave Stimulation of Excitable *Cells. Biophys J* **2013**, *104(12)*, pp 2622-8. DOI: https://www.sciencedirect.com/science/article/pii/S0006349513005705?via%3Dihub
13. Curecheriu L, Foca-Nici E, Vlahovici AL, Avadane O, Sandu DD, Creangai D, Miclaus S. Radiofrequency wave effects on DNA and RNA levels in some animal tissues. *Rom. Journ Phys* **2007**, *52(3–4)*, pp 389–395. DOI: http://www.nipne.ro/rjp/2007_52_3-4/0389_0395.pdf
14. Titushkin IA, Rao VS, Pickard WF, Moros EG, Shafirstein G, Cho MR. Altered Calcium Dynamics Mediates P19-Derived Neuron-Like Cell Responses to Millimeter-Wave Radiation. *Radiat Res* **2009**, *172(6)*, pp 725–736. DOI: https://www.ncbi.nlm.nih.gov/pubmed/19929419Bock J, Fukuyo Y, Kang S, Phipps ML, Alexandrov LB, Rasmussen KØ, Bishop AR, Rosen ED, Martinez JS, Chen HT, Rodriguez G, Alexandrov BS, Usheva A. Mammalian Stem Cells Reprogramming in Response to Terahertz Radiation. *PLoS One* [Internet]. **2010**; *e15806*. DOI: https://journals.plos.org/plosone/article?id=10.1371/journal.pone.0015806
15. Komoshvili K, Levitan J, Aronov S, Kapilevich B, Yahalom A. Millimeter waves non-thermal effect on human lung cancer cells. IEEE International Conference on Microwaves, Communications, Antennas and Electronic Systems - COMCAS 2011; 2011 November 7-9; Tel Aviv, Israel. 1-4 p. DOI: https://ieeexplore.ieee.org/document/6105865
16. Homenko A, Kapilevich B, Kornstein R, Firer M. Effects of 100 GHz radiation on alkaline phosphatase activity and antigen–antibody interaction. *Bioelectromagnetics* **2009**, *30(3)*, pp 167–175. DOI: https://onlinelibrary.wiley.com/doi/abs/10.1002/bem.20466
17. Beneduci A, Chidichimo G, Triprepi S, Perrotta E. Transmission Electron Microscopy Study of the Effects Produced by Wide-band Low-power Millimeter Waves on MCF-7 Human Breast Cancer Cells in Culture. *Anticancer Res* **2005**, *25(2A)*, pp 1009–1013. DOI: http://ar.iiarjournals.org/content/25/2A/1009.long
18. Grenier K, Dubuc D, Chen T, Artis F, Chretiennot T, Poupot M, Fournie JJ. Recent advances in microwave-based dielectric spectroscopy at the cellular level for cancer investigations. *IEEE Trans Microw Theory Tech* **2013**, *61(5)*, pp 2023–2030. DOI: https://hal.archives-ouvertes.fr/hal-00879581/document
19. Prohofsky EW, Eyster JM. Prediction of giant breathing and rocking modes in double helical RNA. *Phys Lett* **1974**, *50A(5)*, pp 329–330. DOI: https://pdf.sciencedirectassets.com/271541/
20. Grundler W, Keilmann F, Fröhlich H. Resonant growth rate response of yeast cells irradiated by weak microwaves. *Phys Lett A* **1977**, *62(6)*, pp 463–466. DOI: https://doi.org/10.1016/0375-9601(77)90696-X
21. Fröhlich H. Coherent Processes in Biological Systems. *J Am Chem Soc* **1980**, *157*, pp 47.
22. Belyaev IY, Alipov YD, Polunin VA, Shcheglov VS. Evidence for Dependence of Resonant Frequency of Millimeter Wave Interaction with *Escherichia coli* K12 Cells on Haploid Genome Length. *Electro- and Magnetobiology* **1993**, *12(1)*, pp 39–49. DOI: https://www.tandfonline.com/doi/abs/10.3109/15368379309012861
23. Wao H, Mhaskar R, Kumar A, Miladinovic B, Djulbegovic B. Survival of patients with non-small cell lung cancer without treatment: a systematic review and meta-analysis. *Syst Rev* [Internet]. **2013**; *2*, pp 10. DOI: https://systematicreviewsjournal.biomedcentral.com/articles/10.1186/2046-4053-2-10
24. Burrell RA, Swanton C. Tumour heterogeneity and the evolution of polyclonal drug resistance. *Mol Oncol* **2014**, *8(6)*, pp 1095–1111. DOI: https://febs.onlinelibrary.wiley.com/doi/full/10.1016/j.molonc.2014.06.005
25. Saraste A, Pulkki K. Morphologic and biochemical hallmarks of apoptosis. *Cardiovascular Research* **2000**, *45(3)*, pp 528–537. DOI: https://academic.oup.com/cardiovascres/article/45/3/528/304427
26. Cho KA, Ryu SJ, Oh YS, Park JH, Lee JW, Kim HP, Kim KT, Jang IS, Park SC. Morphological adjustment of senescent cells by modulating caveolin-1 status. *J Biol Chem* **2004**, *279(40)*, pp 42270-8. DOI: https://www.jbc.org/content/279/40/42270

27. Bharadwaj D, Mandal M. Senescence in polyploid giant cancer cells: A road that leads to chemoresistance. *Cytokine Growth Factor Rev* **2020**, *52*, pp 68-75. DOI: https://www.sciencedirect.com/science/article/pii/S1359610119300899?via%3Dihub
28. Helmy IM, Abdel Azim AM. Efficacy of ImageJ in the assessment of apoptosis. *Diagn Pathol* **2012**, *7*, pp 15. DOI: https://diagnosticpathology.biomedcentral.com/articles/10.1186/1746-1596-7-15
29. Liu N, Wang YA, Sun Y, Ecsedy J, Sun J, Li X, Wang P. Inhibition of Aurora A enhances radiosensitivity in selected lung cancer cell lines. *Respir Res* [Internet]. **2019**, *20*, pp 230. DOI: https://respiratory-research.biomedcentral.com/articles/10.1186/s12931-019-1194-8
30. Hernandez-Segura A, Nehme J, Demaria M. Hallmarks of Cellular Senescence. *Trends Cell Biol* **2018**, *28(6)*, pp 436-453. DOI: https://www.sciencedirect.com/science/article/pii/S0962892418300205?via%3Dihub
31. Conlon I, Raff M. Size control in animal development. *Cell* **1999**, *96(2)*, pp 235-44. DOI: https://www.sciencedirect.com/science/article/pii/S0092867400805632?via%3Dihub
32. Zhadobov M, Chahat N, Sauleau R, Le Quement C, Le Drean Y. Millimeter-wave interactions with the human body: State of knowledge and recent advances. *International Journal of Microwave and Wireless Technologies* **2011**, *3(2)*, pp 237-247. DOI: https://doi.org/10.1017/S1759078711000122
33. Apollonio F, Liberti M, Paffi A, Merla C, Marracino P, Denzi A, Marino C, d'Inzeo G. Feasibility for Microwaves Energy to Affect Biological Systems Via Nonthermal Mechanisms: A Systematic Approach. *IEEE Trans Microw Theory Tech* **2013**, *61(5)*, pp 2031-2045. DOI: https://ieeexplore.ieee.org/document/6478850
34. Hayflick L. The limited in vitro lifetime of human diploid cell strains. *Exp Cell Res* **1965**, *37*, pp 614-36. DOI: https://www.sciencedirect.com/science/article/pii/0014482765902119
35. Kim KS, Cho CH, Park EK, Jung MH, Yoon KS, Park HK. AFM-detected apoptotic changes in morphology and biophysical property caused by paclitaxel in Ishikawa and HeLa cells. *PLoS One* [Internet]. **2012**, *7(1)*, e30066. DOI: https://journals.plos.org/plosone/article?id=10.1371/journal.pone.0030066
36. Osborne LD, Li GZ, How T, O'Brien ET, Blobe GC, Superfine R, Mythreye K. TGF-β regulates LARG and GEF-H1 during EMT to affect stiffening response to force and cell invasion. *Mol Biol Cell* **2014**, *25(22)*, pp 3528-40. DOI: https://www.ncbi.nlm.nih.gov/pmc/articles/PMC4230614/
37. Lin HH, Lin HK, Lin IH, Chiou YW, Chen HW, Liu CY, Harn HI, Chiu WT, Wang YK, Shen MR, Tang MJ. Mechanical phenotype of cancer cells: cell softening and loss of stiffness sensing. *Oncotarget* **2015**, *6(25)*, pp 20946-58. DOI: https://www.oncotarget.com/article/4173/
38. Raudenska M, Kratochvilova M, Vicar T, Gumulec J, Balvan J, Polanska H, Pribyl J, Masarik M. Cisplatin enhances cell stiffness and decreases invasiveness rate in prostate cancer cells by actin accumulation. *Sci Rep* [Internet]. **2019**, *9*, pp 1660. DOI: https://www.nature.com/articles/s41598-018-38199-7
39. Roberson RS, Kussick SJ, Vallieres E, Chen SY, Wu DY. Escape from therapy-induced accelerated cellular senescence in p53-null lung cancer cells and in human lung cancers. *Cancer Res* **2005**, *65(7)*, pp 2795-803. DOI: https://cancerres.aacrjournals.org/content/65/7/2795.long
40. Logani MK, Szabo I, Makar V, Bhanushali A, Alekseev S, Ziskin MC. Effect of millimeter wave irradiation on tumor metastasis. *Bioelectromagnetics* **2006**, *27(4)*, pp 258-64. DOI: https://onlinelibrary.wiley.com/doi/abs/10.1002/bem.20208